J. Fluid Mech. (1995), *vol.* 299, *pp.* 73–95

Liquid-metal flow in a system of electrically coupled U-bends in a strong uniform magnetic field

By SERGEI MOLOKOV† AND ROBERT STIEGLITZ

Forschungszentrum Karlsruhe GmbH, Institut für Angewandte Thermo- und Fluiddynamik, Postfach 36 40, D-76021 Karlsruhe, Germany

(Received 14 November 1994 and in revised form 26 April 1995)

Liquid-metal magnetohydrodynamic flow in a system of electrically coupled U-bends in a strong uniform magnetic field is studied. The ducts composing the bends are electrically conducting and have rectangular cross-sections. It has been anticipated that very strong global electric currents are induced in the system, which modify the flow pattern and produce a very high pressure drop compared to the flow in a single U-bend. A detailed asymptotic analysis of flow for high values of the Harmann number (in fusion blanket applications of the order of 10^3–10^4) shows that circulation of global currents results in several types of peculiar flow patterns. In ducts parallel to the magnetic field a combination of helical and recirculatory flow types may be present and vary from one bend to another. The magnitude of the recirculatory motion may become very high depending on the flow-rate distribution between the bends in the system. The recirculatory flow may account for about 50% of the flow in all bends. In addition there are equal and opposite jets at the walls parallel to the magnetic field, which are common to any two bends. The pressure drop due to three-dimensional effects linearly increases with the number of bends in a system and may significantly affect the total pressure drop. To suppress this and some other unwelcome tendencies either the ducts perpendicular to the magnetic field should be electrically separated, or the flow direction in the neighbouring ducts should be made opposite, so that leakage currents cancel each other.

1. Introduction

In many applications of magnetohydrodynamics, such as electromagnetic pumping, flow coupling, energy conversion, etc., an electrically conducting fluid flows in a system of ducts rather than in a single duct. If ducts are electrically separated from each other, for example by means of electrical insulation of the duct walls or using insulating ceramic layers inside the electrically conducting walls (so-called flow channel inserts, Malang *et al.* 1988), electric currents induced in one duct are confined to it, so that each duct may be treated individually. On the other hand, in the absence of electrical separation currents induced in one duct may enter the other ducts via common electrically conducting walls and affect the flow in the whole system. These electric currents are called the global currents (Madarame, Taghavi & Tillack 1985).

In some situations this effect may be very significant and even dominant. A prominent example is provided by two toroidal concepts of self-cooled liquid-metal blankets for tokamak fusion reactors (Smith *et al.* 1985; Malang *et al.* 1988). A

† Present address: University of Oxford, Department of Engineering Science, 19, Parks Road, Oxford OX1 3PJ, UK.

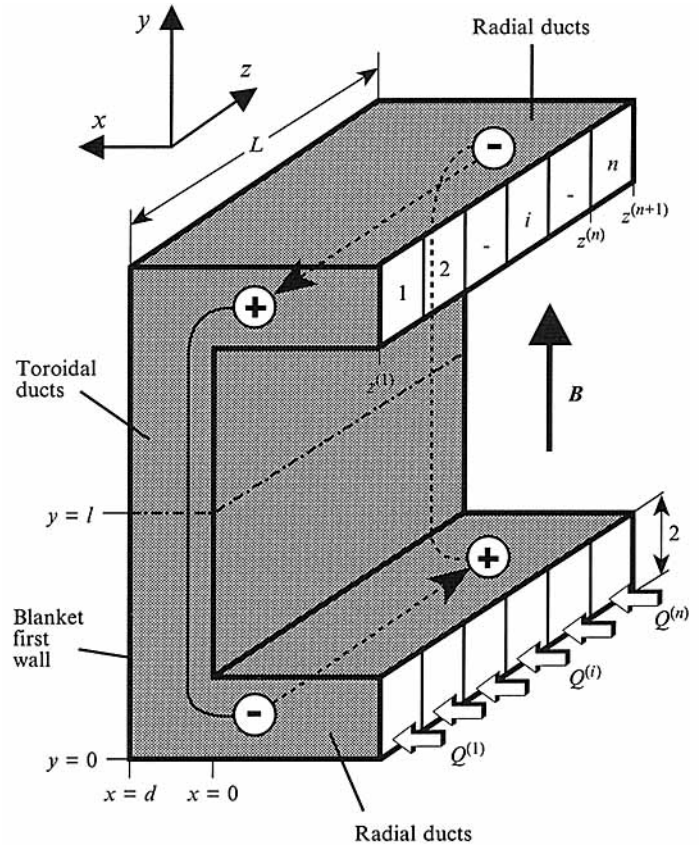

FIGURE 1. Schematic diagram of a toroidal liquid-metal blanket concept: flow in a system of electrically coupled U-bends. The blanket first wall is at $x = d$.

simplified schematic diagram of the blanket is shown in figure 1. The geometry consists of the so-called toroidal ducts, which are aligned with the main component of a strong magnetic field, and two sets of radial ducts, which supply liquid metal to and remove it from the toroidal ducts. The radial ducts are perpendicular to the magnetic field. Thus an electrically conducting fluid, which cools the plasma facing first wall, flows in a system of U-bends. The U-bends have common walls parallel to the magnetic field. If these walls are electrically conducting, global electric currents may circulate in the whole system of bends, affecting both the flow structure and the pressure drop, the characteristics of great importance for fusion blanket applications.

The significance of global current effects is due to the magnitude of three-dimensional currents (the currents due to three-dimensional effects) induced in the U-bend geometry. If the dividing walls are removed, a system of U-bends becomes a wide single U-bend. In such a bend a very high voltage difference between the sidewalls of the radial ducts is induced. This difference is proportional to the duct width L (for more details see §4.2). Owing to the opposite flow direction in the two radial ducts, the induced voltage for $y < l$ and for $y > l$ is of opposite sign (see figure 1). This voltage may shortcut between the radial ducts along conducting walls or inside the fluid and cause very strong global currents producing a large pressure drop. The presence of the dividing walls complicates the problem since these walls provide additional paths for the electric current. The importance of the global currents for fusion blanket

applications was shown first by Madarame *et al.* (1985) on the basis of a very simplified flow model.

The present paper treats the three-dimensional flow in a system of n U-bends under the following assumptions (cf. Hua *et al.* 1988; Moon & Walker 1990; Molokov & Bühler 1994) (i) the induced magnetic field may be neglected (small magnetic Reynolds number); (ii) the applied magnetic field is strong ($M \gg 1$, $N \gg M^{3/2}$), so that viscous effects are confined to thin layers and inertia forces can be neglected everywhere. Here $M = B_0 a(\sigma/\rho\nu)^{1/2}$ is the Hartmann number and $N = \sigma a B_0^2/\rho\nu_0$ is the interaction parameter, where σ, ρ, ν are the electrical conductivity, density and kinematic viscosity of the fluid, B_0 is the induction of the applied constant magnetic field, ν_0 is the characteristic velocity, and the characteristic length a is half the distance between tops and bottoms of the radial ducts. In fusion blanket applications $M = 10^3$–10^4 and $N = 10^2$–10^5; (iii) electrically conducting walls are much better conductors than all the boundary and internal layers ($c \gg M^{-1/2}$), so that currents conducted by the layers are neglected. Here $c = \sigma_w t_w/\sigma a$ is the wall conductance ratio, where σ_w and t_w are the wall conductivity and thickness; (iv) radial ducts are semi-infinite, so that the flow is fully developed as $x \to -\infty$.

The flow in a single U-bend ($n = 1$) has been considered by Molokov & Bühler (1994) (hereinafter referred to as MB94) under the assumptions listed above. In a strong magnetic field, in both radial and toroidal ducts there are cores and boundary layers at all duct walls (figure 2). At walls parallel to the magnetic field the layers, which are called parabolic ones due to the nature of the equations governing the flow there, have thickness $O(M^{-1/2})$. They carry non-zero volume flux in jets with velocity $O(M^{1/2})$. In the cores of both the radial and toroidal ducts the fluid flows perpendicular to the magnetic field. The two cores are separated by the internal layer at $x = 0$. In the radial duct part of the flow is carried by the core, while the other part is carried by the layers at walls 5 and 8 (wall numbers are shown in figure 2). When the fluid approaches the toroidal duct from the radial one it meets an internal layer at $x = 0$, which for the fluid appears to be a permeable wall. Part of the fluid flows around this layer along the layers at the sidewalls 5 and 8 or upward in the internal layer to enter the layer at wall 2. The other part crosses the internal layer, penetrates into the core of the toroidal duct, flows in planes perpendicular to the magnetic field toward the walls 1, 3 and 9 and enters the parabolic layers at these walls. In the toroidal duct all the volume flux is carried by parabolic layers at walls 1, 2, 3 and 9 by high-velocity jets, since the y-component of the core velocity vanishes. The flow distribution between the layers in the toroidal duct varies with y. The volume fluxes carried by the layers at walls 1, 3 and 9 and by the internal layer at $x = 0$ for $0 < y < 2$ monotonically increase with y, while that carried by the layer at wall 2 monotonically decreases with y. Under certain circumstances the flow in the latter may become reversed, which leads to a recirculatory flow in a part of the toroidal duct. In addition there is mass exchange between the parabolic layers at walls 1, 2, 3 and 9 through the corners $A1$–$A4$, so that flow patterns of a helical type may be present. A number of qualitatively different flow patterns which may occur for certain range of the wall conductance ratio and the toroidal-duct aspect ratio d, have been presented in MB94.

Electrical coupling of the parallel channels brings new effects. Molokov (1993) considered the flow in a system of electrically coupled straight thin-walled rectangular ducts, which corresponds to that in the radial ducts as $x \to -\infty$. The assumptions were less restrictive than in this paper. It has been shown that even in straight ducts the flow pattern may involve forward and backward jets if the pressure gradients in individual ducts are not equal. Since the flow pattern in a system of U-bends contains features of

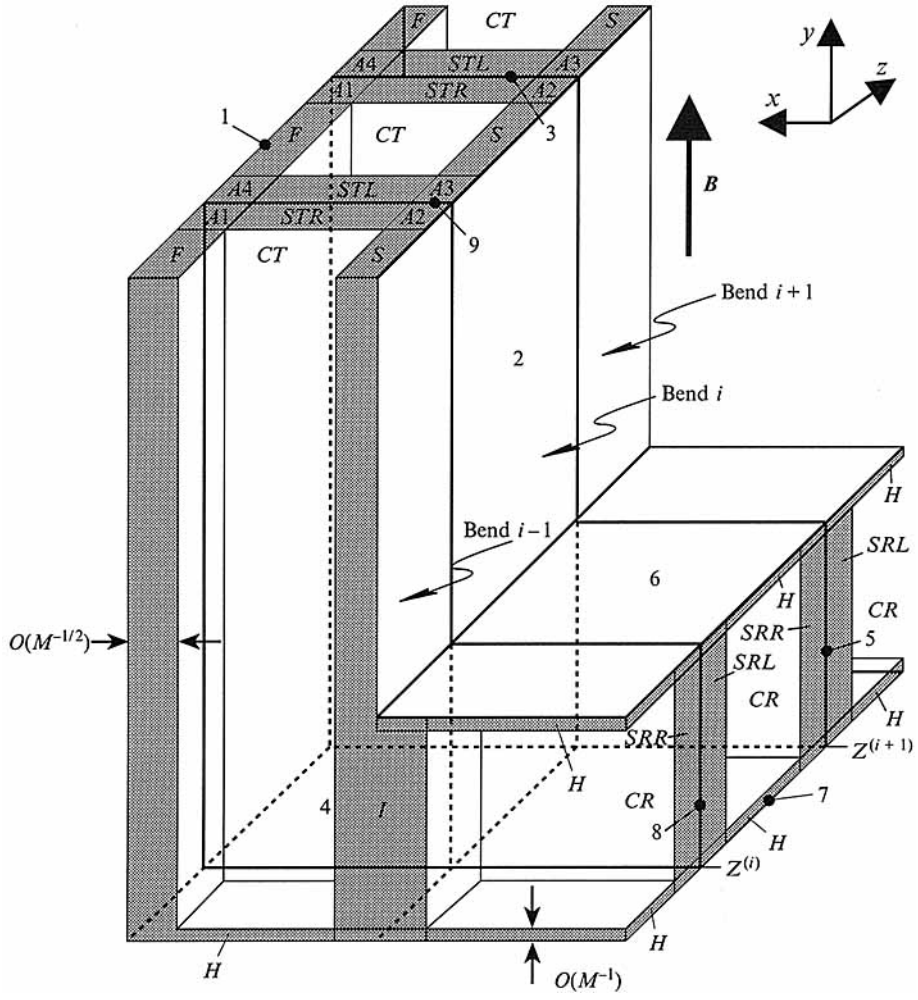

FIGURE 2. Flow subregions for $M \gg 1$ and wall numbers of bend i for $y < l$. The walls are: blanket first and second walls (1, 2); sidewalls of the toroidal (3, 9) and the radial (5, 8) ducts; top and bottom of the radial duct (6, 7); bottom of the toroidal duct (4). Flow subregions are: *CR*, *CT* – cores of the radial and toroidal ducts, *H* – the Hartmann layers, *F*, *S*, *I*, *SRL*, *SRR*, *STL*, *STR* – the parabolic layers, *A*1–*A*4 – the corner layers.

both the flow in a single U-bend and that in electrically coupled straight ducts, the resulting flow structures are even more complicated.

2. Formulation

Consider the steady isothermal flow of a viscous conducting incompressible fluid in a system of n electrically coupled U-bends (see figure 1). Each U-bend is composed of two radial ducts perpendicular to the external magnetic field $\boldsymbol{B} = B_0 \hat{\boldsymbol{y}}$, and a toroidal duct parallel to the field. All ducts have rectangular cross-sections. The radial ducts are semi-infinite, so that far away from the junction $x = 0$ the flow is fully developed. The system of U-bends is symmetric with respect to the plane $y = l$, and since inertia is assumed to play no role, the flow in a half of the system $y < l$ is considered under appropriate symmetry conditions.

Consider the flow in a U-bend i. The walls of this bend are numbered from 1 to 9, as shown in figure 2. The sidewalls are at $z = z^{(i)}$ $(i = 1, \ldots, n+1)$; $z^{(1)} = 0$, $z^{(n+1)} = L$. The dividing walls 8 and 9 for bend i $(i \neq 1)$ coincide with walls 5 and 3 for bend $i-1$, respectively. The dimensionless inertialess inductionless equations governing the flow in bend i are (e.g. MB94)

$$M^{-2}\nabla^2 \boldsymbol{v}^{(i)} + \boldsymbol{j}^{(i)} \times \hat{\boldsymbol{y}} = \nabla p^{(i)}, \quad \boldsymbol{j}^{(i)} = -\nabla \phi^{(i)} + \boldsymbol{v}^{(i)} \times \hat{\boldsymbol{y}}, \tag{1a, b}$$

$$\nabla \cdot \boldsymbol{v}^{(i)} = 0, \quad \nabla \cdot \boldsymbol{j}^{(i)} = 0. \tag{1c, d}$$

The fluid velocity $\boldsymbol{v}^{(i)}$, the electric current density $\boldsymbol{j}^{(i)}$, the electric potential $\phi^{(i)}$ and the pressure $p^{(i)}$ are normalized by v_0, $v_0 B_0 \sigma$, $v_0 B_0 a$ and $\sigma v_0 B_0^2 a$, respectively. The boundary conditions at each wall of bend i are the no-slip condition

$$\boldsymbol{v}^{(i)} = 0 \tag{1e}$$

and the thin-wall conditions (e.g. Hua & Picologlou 1991)

$$j_z^{(i)} - j_z^{(i+1)} = c_k^{(i)} \nabla_k^2 \phi_k^{(i)} \quad \text{for} \quad k = 3, 5 (i \neq n), \tag{1f}$$

$$j_z^{(i-1)} - j_z^{(i)} = c_k^{(i)} \nabla_k^2 \phi_k^{(i)} \quad \text{for} \quad k = 8, 9 (i \neq 1), \tag{1g}$$

$$\boldsymbol{j}^{(i)} \cdot \hat{\boldsymbol{n}}_k = c_k^{(i)} \nabla_k^2 \phi_k^{(i)} \quad \text{for all other walls.} \tag{1h}$$

Here $\hat{\boldsymbol{n}}_k$ is the inward normal unit vector to wall k; $c_k^{(i)} = \sigma_k^{(i)} t_k^{(i)} / \sigma a$ is the wall conductance ratio; $\sigma_k^{(i)}$ and $t_k^{(i)}$ are the electrical conductivity and thickness of wall k, respectively; ∇_k^2 is the Laplacian in the plane of wall k; $\phi_k^{(i)}$ is the wall potential equal to the fluid potential on wall k; $\phi_8^{(i)} = \phi_5^{(i-1)}$, $\phi_9^{(i)} = \phi_3^{(i-1)}$ for $i \neq 1$.

The symmetry conditions are

$$\phi^{(i)} = p^{(i)} = 0 \quad \text{at} \quad y = l. \tag{1i}$$

In the radial ducts, far from the junction, the flow is fully developed, so that

$$\frac{\partial \phi^{(i)}}{\partial x} = \frac{\partial p^{(i)}}{\partial y} = \frac{\partial p^{(i)}}{\partial z} = 0 \quad \text{as} \quad x \to -\infty. \tag{1j}$$

The characteristic velocity v_0 is defined as an average velocity in the whole system, i.e.

$$\sum_{i=1}^{n} Q^{(i)} = 2L. \tag{1k}$$

The total flow rate is $Q = 2L$ and the flow rates $Q^{(i)}$ in individual bends are

$$Q^{(i)} = \int_0^2 \mathrm{d}y \int_{z^{(i)}}^{z^{(i+1)}} v_x^{(i)}(x, y, z)\, \mathrm{d}z \quad \text{for any} \quad x \leqslant 0. \tag{1l}$$

3. Flow analysis at high Hartmann numbers

At high Hartmann numbers the flow exhibits the following subregions (figure 2): the inviscid cores of the radial and toroidal ducts *CR* and *CT*, the Hartmann boundary layers *H* near the walls perpendicular to the magnetic field with a thickness $O(M^{-1})$, the parabolic layers with a thickness $O(M^{-1/2})$, the corner layers *A*1–*A*4 with dimensions $O(M^{-1/2}) \times O(M^{-1/2})$. The parabolic layers are at the sidewalls of both radial and toroidal ducts (*SRL*, *SRR*, *STL* and *STR*), at the first wall (*F*), at the second wall (*S*), and the internal layer *I* at $x = 0$. Layers *I* and *S* merge at $y = 2$. Corner layers *A*1–*A*4 are formed at intersections of the parabolic layers.

Following the analysis of MB94 the problem (1) is reduced to a system of equations governing the wall potentials $\phi_k^{(i)}$ and the core pressures $p_{CR}^{(i)}(x,z)$:

$$c_5^{(i)}\nabla_5^2\phi_5^{(i)} = -\frac{\partial p_{CR}^{(i+1)}}{\partial x}(x, z = z^{(i+1)}) + \frac{\partial p_{CR}^{(i)}}{\partial x}(x, z = z^{(i+1)}) \quad \text{for} \quad i \neq n, \tag{2a}$$

$$c_5^{(n)}\nabla_5^2\phi_5^{(n)} = \frac{\partial p_{CR}^{(n)}}{\partial x}(x, z = z^{(n+1)}), \tag{2b}$$

$$c_8^{(1)}\nabla_8^2\phi_8^{(1)} = -\frac{\partial p_{CR}^{(1)}}{\partial x}(x, z = z^{(1)}), \tag{2c}$$

$$c_7^{(i)}\nabla_7^2\phi_7^{(i)} = \tfrac{1}{2}(\phi_7^{(i)} - \phi_6^{(i)}), \tag{2d}$$

$$c_6^{(i)}\nabla_6^2\phi_6^{(i)} = -\tfrac{1}{2}(\phi_7^{(i)} - \phi_6^{(i)}), \tag{2e}$$

$$\nabla_{xz}^2 p_{CR}^{(i)} = 0, \tag{2f}$$

$$\nabla_1^2\phi_1^{(i)} = \nabla_2^2\phi_2^{(i)} = \nabla_3^2\phi_3^{(i)} = \nabla_9^2\phi_9^{(1)} = 0, \tag{2g–j}$$

$$lc_4^{(i)}\nabla_4^2\phi_4^{(i)} = \phi_4^{(i)}, \tag{2k}$$

$$\int_0^2 \{\phi_5^{(i)}(x,y) - \phi_8^{(i)}(x,y)\}\,\mathrm{d}y - 2\int_{z^{(i)}}^{z^{(i+1)}} \frac{\partial p_{CR}^{(i)}}{\partial x}(x,z)\,\mathrm{d}z = Q^{(i)} \quad \text{for} \quad x \leqslant 0, \tag{2l}$$

$$\phi_8^{(i)} = \phi_5^{(i-1)}, \quad \phi_9^{(i)} = \phi_3^{(i-1)} \quad \text{for} \quad i \neq 1, \tag{2m,n}$$

where ∇_{xz} is the vector gradient in the plane (x,z). In the above i varies from 1 to n.

Consider the boundary conditions for system (2). On the interface between the walls and at the junction $x = 0$ the wall electric potential is continuous. In addition, Kirchhoff's law applies for components of the wall electric currents normal to the interface. If Γ_{kmj} is the common boundary of three walls k, m and j (wall j belongs to a neighbouring bend $i-1$ or $i+1$ and is equal to either k or m), the conditions are:

$$\phi_k^{(i)} = \phi_m^{(i)} = \phi_j^{(i\pm1)}, \tag{3a}$$

$$c_k^{(i)}\frac{\partial\phi_k^{(i)}}{\partial s_k} + c_m^{(i)}\frac{\partial\phi_m^{(i)}}{\partial s_m} + c_j^{(i\pm1)}\frac{\partial\phi_j^{(i\pm1)}}{\partial s_j} = 0, \tag{3b}$$

where $\hat{s}_k$, $\hat{s}_m$ and $\hat{s}_j$ are outward normal vectors to Γ_{kmj} in the planes of walls k, m and j, respectively.

If only two walls k and m intersect, the conditions (3a,b) reduce to

$$\phi_k^{(i)} = \phi_m^{(i)}, \quad c_k^{(i)}\frac{\partial\phi_k^{(i)}}{\partial s_k} = -c_m^{(i)}\frac{\partial\phi_m^{(i)}}{\partial s_m}. \tag{4a, b}$$

As $x \to -\infty$, the flow becomes fully developed. This gives

$$\frac{\partial\phi_5^{(i)}}{\partial x} = \frac{\partial\phi_6^{(i)}}{\partial x} = \frac{\partial\phi_7^{(i)}}{\partial x} = \frac{\partial\phi_8^{(i)}}{\partial x} = \frac{\partial p_{CR}^{(i)}}{\partial z} = 0. \tag{5}$$

The symmetry conditions are

$$\phi_1^{(i)} = \phi_2^{(i)} = \phi_3^{(i)} = \phi_9^{(i)} = 0 \quad \text{at} \quad y = l. \tag{6}$$

Equations (2)–(6) constitute the problem for the wall potentials and the core pressures in the radial ducts. It should be stressed that this system involves two-dimensional equations only, while the original problem is three-dimensional. Once the

problem (2)–(6) is solved, the other variables in cores CR and CT can be expressed in terms of $\phi_k^{(i)}$ and $p_{CR}^{(i)}$ as follows:

$$\boldsymbol{v}_{CR}^{(i)} = -\boldsymbol{\nabla}_{xz} p_{CR}^{(i)} + \hat{\boldsymbol{y}} \times \boldsymbol{\nabla}_{xz} \phi_{CR}^{(i)}, \quad \boldsymbol{v}_{CT}^{(i)} = \hat{\boldsymbol{y}} \times \boldsymbol{\nabla}_{xz} \phi_{CT}^{(i)}, \tag{7a, b}$$

$$\phi_{CR}^{(i)} = \phi_6^{(i)} + (1 - \tfrac{1}{2}y)[\phi_7^{(i)} - \phi_6^{(i)}], \quad \phi_{CT}^{(i)} = (1 - yl^{-1})\,\phi_4^{(i)}, \tag{7c, d}$$

$$\boldsymbol{j}_{CR}^{(i)} = \tfrac{1}{2}[\phi_7^{(i)} - \phi_6^{(i)}]\,\hat{\boldsymbol{y}} + \hat{\boldsymbol{y}} \times \boldsymbol{\nabla}_{xz} p_{CR}^{(i)}, \quad \boldsymbol{j}_{CT}^{(i)} = l^{-1}\phi_4^{(i)}\hat{\boldsymbol{y}}, \quad p_{CT}^{(i)} = 0. \tag{7e–g}$$

Equations (7) demonstrate certain specific features of the flow in the *toroidal* duct of bend i. They are (i) the core CT does not carry volume flux in the y-direction, so that all the volume flux is carried by the parabolic layers; (ii) the electric potential $\phi_{CT}^{(i)}$ is a streamfunction for the core velocity. The fluid in the core flows in the (x, z)-plane, i.e. perpendicular to the magnetic field following the isolines of $\phi_4^{(i)}(x, z)$, the latter being responsible for the flow distribution among the parabolic layers in the whole toroidal duct (the so-called pumping effect, cf. MB94); (iii) owing to the symmetry, the core potential and the core velocity vanish at $y = l$; (iv) the core current flows only along magnetic field lines, i.e. there is no path of electric current from the radial duct to the toroidal duct within the fluid to the leading order; (v) the pressure in the core is zero to the leading order, i.e. there is no pressure drop in the toroidal ducts.

Similar to the core, all local and global flow variables in the layers can be expressed in terms of the wall potentials and the core pressures. The Hartmann layers have a well-known exponential structure. They are not considered here and neither are the corner layers $A1$–$A4$, which are unable to carry volume flux in the y-direction. The parabolic boundary and interior layers are treated integrally with the most essential information about them given by the so-called local flow rates. In what follows we first exclude from the consideration layers S and I, which will be treated later separately.

Consider an arbitrary parabolic layer P in bend i at a wall k parallel to the magnetic field ($k = 1, 3, 5, 8, 9$). Let us introduce a local Cartesian coordinate system based on unit vectors $\hat{\boldsymbol{t}}_k$, $\hat{\boldsymbol{y}}$, $\hat{\boldsymbol{n}}_k$, where $\hat{\boldsymbol{t}}_k = \hat{\boldsymbol{y}} \times \hat{\boldsymbol{n}}_k$, with the origin at the bottom of wall k at $y = 0$. In the layer $\boldsymbol{v}^{(i)} = M^{1/2}\boldsymbol{v}_P^{(i)}$, $p^{(i)} = p_C^{(i)} + M^{-1/2}p_P^{(i)}$, where index C denotes the core adjacent to wall k; all quantities with index P are $O(1)$. In layer P the following equations and boundary conditions hold:

$$\frac{\partial^2 p_P^{(i)}}{\partial \xi_k^2} = \frac{\partial (\boldsymbol{v}_P^{(i)} \cdot \hat{\boldsymbol{y}})}{\partial y}, \quad \boldsymbol{v}_P^{(i)} \cdot \hat{\boldsymbol{t}}_k = \frac{\partial \phi_P^{(i)}}{\partial \xi_k}, \tag{8a, b}$$

$$\boldsymbol{v}_P^{(i)} \cdot \hat{\boldsymbol{y}} = 0 \quad \text{at} \quad y = 0, \tag{8c}$$

$$\frac{\partial p_P^{(i)}}{\partial \xi_k} = \frac{\partial \phi_k^{(i)}}{\partial t_k}, \quad \phi_P^{(i)} = \phi_k^{(i)} \quad \text{at} \quad \xi_k = 0, \tag{8d, e}$$

$$\frac{\partial p_P^{(i)}}{\partial \xi_k} \to \frac{\partial p_C^{(i)}}{\partial n_k}(n_k = 0), \quad \phi_P^{(i)} \to \phi_C^{(i)}(n_k = 0) \quad \text{as} \quad \xi_k \to \infty. \tag{8f, g}$$

Here $\xi_k = M^{1/2} n_k$ is the stretched boundary-layer variable. The other equations and the boundary conditions which hold in the parabolic layer are not important for an integral analysis.

Integrating (8a, b) and using the boundary conditions (8c–g) gives the expressions for the local flow rates $q_{P,t}^{(i)}$ and $q_{P,y}^{(i)}$ carried by the layer in the directions $\hat{\boldsymbol{t}}_k$ and $\hat{\boldsymbol{y}}$, respectively:

$$q_{P,t}^{(i)} = \int_0^\infty \boldsymbol{v}_P^{(i)} \cdot \hat{\boldsymbol{t}}_k \, \mathrm{d}\xi_k = \phi_C^{(i)}(n_k = 0) - \phi_k^{(i)}, \tag{9a}$$

$$q_{P,y}^{(i)} = \int_0^\infty \boldsymbol{v}_P^{(i)} \cdot \hat{\boldsymbol{y}} \, \mathrm{d}\xi_k = y \frac{\partial p_C^{(i)}}{\partial n_k}(n_k = 0) + \int_0^y \frac{\partial \phi_k^{(i)}}{\partial t_k} \mathrm{d}y. \tag{9b}$$

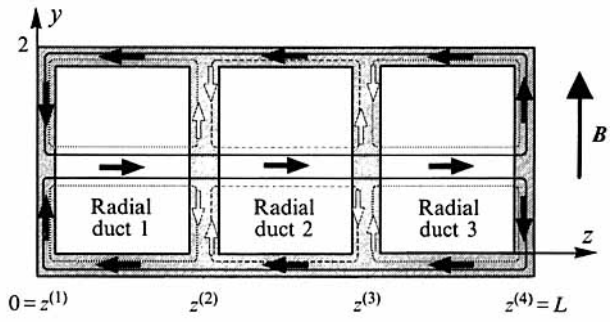

FIGURE 3. Integral path of electric currents in radial ducts in the fully developed flow region for $n = 3$.

Using the condition $q^{(i)}_{P,y} = 0$ at $y = 2$ for layers SRL and SRR and equation $(7g)$ for layers F, STL and STR gives

$$\frac{\partial p^{(i)}_C}{\partial n_k}(n_k = 0) = \begin{cases} -\frac{1}{2}\int_0^2 \frac{\partial \phi^{(i)}_k}{\partial t_k}\,\mathrm{d}y & \text{for} \quad k = 5, 8 \\ 0 & \text{for} \quad k = 1, 3, 9. \end{cases} \tag{10}$$

Taking into account the velocity of the fluid entering layer P from the core, namely

$$\boldsymbol{v}^{(i)}_C \cdot \hat{\boldsymbol{n}}_k = -\frac{\partial p^{(i)}_C}{\partial n_k} - \frac{\partial \phi^{(i)}_C}{\partial t_k} \quad \text{at} \quad n_k = 0 \tag{11}$$

completes mass conservation within the layer.

Equation $(9a)$ expresses the well-known fact that the local flow rate carried by the parabolic layer in the direction parallel to the wall and perpendicular to the magnetic field is proportional to the local jump in the electric potential across the layer.

The flow rate $q^{(i)}_{P,y}$ may be expressed in terms of the wall current $j^{(i)}_k$. The latter is

$$j^{(i)}_k = -\frac{\sigma^{(i)}_k}{\sigma} \nabla_k \phi^{(i)}_k. \tag{12}$$

From $(9b)$ and (10) it follows that

$$q^{(i)}_{P,y} = -\frac{\sigma}{\sigma^{(i)}_k} \begin{cases} \int_0^y j^{(i)}_{k,t}\,\mathrm{d}y - \frac{1}{2}y\int_0^2 j^{(i)}_{k,t}\,\mathrm{d}y & \text{for} \quad k = 5, 8 \\ \int_0^y j^{(i)}_{k,t}\,\mathrm{d}y & \text{for} \quad k = 1, 3, 9. \end{cases} \tag{13}$$

For layers F, STR and STL this implies that the amount of fluid carried by them in the y-direction is determined by the current flowing in wall k in the $-\hat{\boldsymbol{t}}_k$-direction integrated from 0 to y, while for layers SRR and SRL the flow rate is determined by the deviation of this current from being linear with y.

Consider the local flow rates carried by the parabolic layers at opposite sides of the dividing walls. Since the wall potential is continuous, by virtue of $(7c, d)$ the core electric potential is continuous across the dividing wall at $z = z^{(i)} (i = 1, \ldots, n)$ as well. Then from (9) and (10) follows that

$$q^{(i)}_{P(-),t} = q^{(i+1)}_{P(+),t}, \quad q^{(i)}_{P(-),y} = -q^{(i+1)}_{P(+),y} \tag{14a, b}$$

for $i = 1, \ldots, n-1$, where the signs $+$ and $-$ refer to the layers P in bends $i+1$ and i, respectively. Given the fact that the direction of $\hat{\boldsymbol{t}}_k$ for layer $P(-)$ is opposite to that for $P(+)$, $(14a, b)$ indicate that the jets at the dividing walls are equal and opposite.

This fact, discussed by Madarame *et al.* (1985) and Molokov (1993) in the context of fully developed flows in straight ducts, is a general property of magnetohydrodynamic flows in rectangular ducts with thin conducting walls.

The jets at the dividing wall k vanish if and only if

$$\phi_k^{(i)} = \phi_C^{(i)}(n_k = 0).$$

If a toroidal duct is concerned, this condition holds for a perfectly conducting dividing wall only. For a radial duct this condition holds in the region of fully developed flow if either the wall is perfectly conducting or the pressure gradients at both sides of the dividing wall are equal. It should be noted that the walls of the radial ducts parallel to the magnetic field may be only partially perfectly conducting. The three-dimensional problem with these walls being perfectly conducting and with fully developed flow conditions as $x \to -\infty$ is unphysical. One would necessarily have to consider the entrance/exit effects, since the three-dimensional currents might flow along these walls with no resistance.

Consider now layers S and I. For layer I the variable ξ_2 varies from $-\infty$ to ∞ so that instead of the boundary conditions (8*d*, *e*) the conditions of matching another core are to be used as $\xi_2 \to -\infty$, which are analogous to (8*f*, *g*). This yields

$$q_{I,z}^{(i)} = \phi_{CR}^{(i)}(x=0) - \phi_{CT}^{(i)}(x=0), \quad q_{I,y}^{(i)} = -y\frac{\partial p_{CR}^{(i)}}{\partial x}(x=0). \qquad (15a,b)$$

In particular, (15*a*) indicates that for $l = 2$ (the so-called 180°-bend) $q_{I,z}^{(i)} = 0$, i.e. all the fluid that enters layer I from the core CR either enters the core CT or flows in the y-direction within layer I so that there is no redistribution of fluid in the z-direction within the layer.

For layer S equation (9*a*) still may be used. Instead of the boundary condition (8*c*) a matching condition with layer I at $y = 2$ is used for determining $q_{S,y}^{(i)}$. This gives

$$q_{S,z}^{(i)} = \phi_2^{(i)} - \phi_{CT}^{(i)}(x=0), \quad q_{S,y}^{(i)} = -2\frac{\partial p_{CR}^{(i)}}{\partial x}(x=0) - \int_2^y \frac{\partial \phi_2^{(i)}}{\partial z}\,\mathrm{d}y. \qquad (16a,b)$$

Total volume fluxes carried by the layers may be obtained by integrating (9), (15*a*, *b*) and (16*a*, *b*).

4. Results and discussion

The system of equations (2) subject to the boundary conditions (3)–(6) is solved numerically. An iterative numerical algorithm to solve equations for a single U-bend ($n = 1$) is described by Molokov & Bühler (1993). To seek the equations governing the flow in a system of U-bends iterations between solutions for single bends are organized. Iterations stop when the differences between nodal pressures and wall potentials between two iteration steps are less than 0.1 %. Results are presented for $c_k^{(i)} = c = 0.4$ for all duct walls and $l = 12$. All ducts have square cross-section ($d = 2$, $z^{(i+1)} - z^{(i)} = 2$), unless otherwise stated explicitly. For simplicity, it is assumed that the system of U-bends is symmetric with respect to the plane $z = \frac{1}{2}L$.

4.1. *Three bends*

To discuss effects caused by the presence of dividing walls on the flow pattern consider the flow in three coupled bends. In each situation two-dimensional effects in the fully developed flow region as $x \to -\infty$ will be discussed first. The quantities describing the flow in this region are called two-dimensional, since none of them, except pressure, varies with x. In the fully developed flow region equations (2)–(6) may be solved

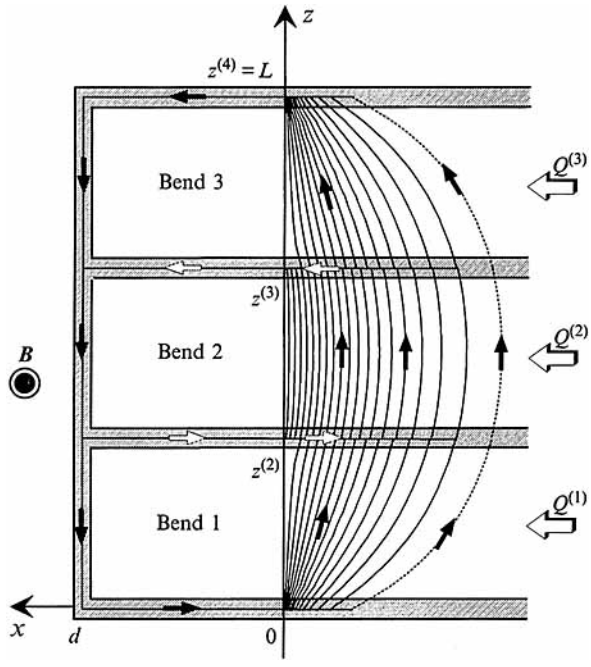

FIGURE 4. Projection of the three-dimensional electric current lines on the (x, z)-plane for $n = 3$, $\gamma = 1$. In the radial ducts these lines are isolines of the three-dimensional pressure.

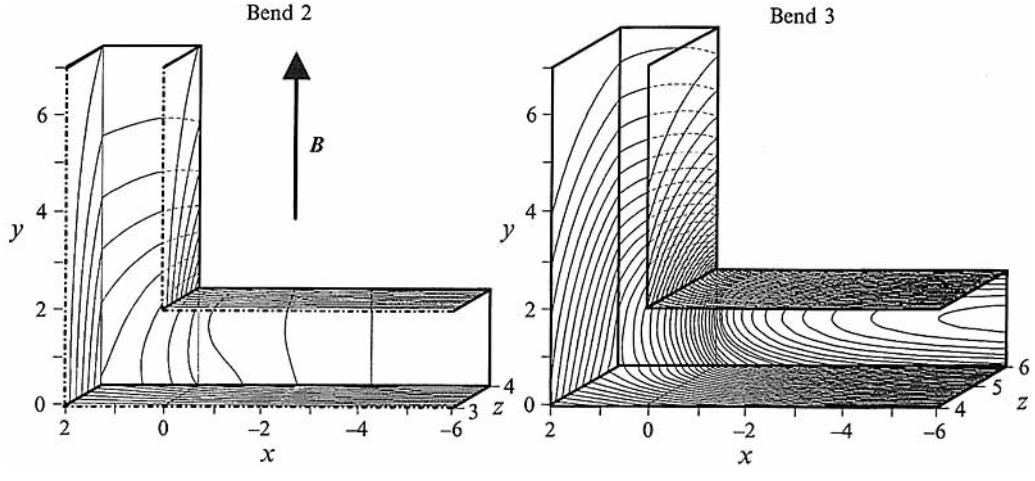

FIGURE 5. Isolines of wall potential in bends 2 and 3 for $n = 3$, $\gamma = 1$. The wall currents flow perpendicular to the isolines. There is almost no variation of the wall potential for $y > 7$.

analytically (Molokov 1993). For bends 2 and 3 the flow distribution between cores CR and layers SRR and SRL is

$$\tilde{Q}^{(i)}_{CR,x} = 2[z^{(i+1)} - z^{(i)}]\frac{1+c}{c}K^{(i)} \quad \text{for} \quad i = 2,3, \quad \tilde{Q}^{(3)}_{SRR,x} = \frac{2}{3c}K^{(3)}, \qquad (17a,b)$$

$$\tilde{Q}^{(2)}_{SRR,x} = -\tilde{Q}^{(3)}_{SRL,x} = \frac{2}{3c}[K^{(2)} - K^{(3)}], \qquad (17c,d)$$

where $K^{(i)} = -\partial p^{(i)}_{CR}/\partial x(x \to -\infty)$ and $\tilde{Q}^{(i)}_{\cdot,x}$ denotes flow rates carried by the radial duct

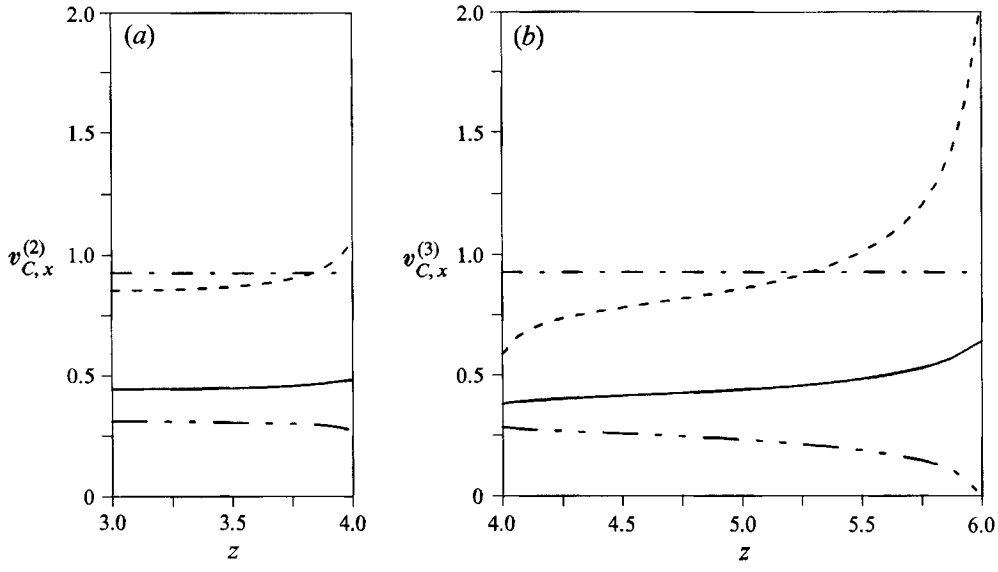

FIGURE 6. Profiles of the x-component of the core velocity at $y = 0$ for $n = 3$, $\gamma = 1$ in (a) bend 2 and (b) bend 3 for $x \to -\infty$ (–·–·–), $x = -0$ (·····), $x = +0$ (——) and $x = d$ (–··–··–).

n	i	$Q^{(i)}$	$\frac{Q^{(i)}_{P,y}(y=l)}{Q^{(i)}}$ (%)	$\frac{Q^{(i)}_{S,y}(y=l)}{Q^{(i)}}$ (%)	$\frac{Q^{(i)}_{STR,y}(y=l)}{Q^{(i)}}$ (%)	$\frac{Q^{(i)}_{STL,y}(y=l)}{Q^{(i)}}$ (%)	$\frac{\partial p^{(i)}_{CR}}{\partial x}(x \to -\infty)$	Δp_{3D}
1	1	4.000	19.4	29.6	25.5	25.5	−0.231	0.147
3	2	3.706	70.2	−1.8	15.8	15.8	−0.265	0.421
	3	4.147	46.0	17.4	50.7	−14.1	−0.265	0.322
9	5	3.897	138.8	−50.6	5.9	5.9	−0.278	1.213
	6	3.897	136.0	−48.6	18.5	−5.9	−0.278	1.176
	7	3.897	126.5	−41.6	33.6	−18.5	−0.278	1.060
	8	3.897	105.7	−26.0	53.9	−33.6	−0.278	0.846
	9	4.361	58.5	13.2	76.5	−48.2	−0.278	0.499

TABLE 1. Main flow characteristics for $n = 1$, 3 and 9 for equal fully developed pressure gradients

cores and layers *SRR*, *SRL* as $x \to -\infty$. The flow in bend 1 may be reconstructed from that in bend 3 by symmetry considerations. The total flow rates are

$$Q^{(2)} = \tilde{Q}^{(2)}_{CR,x} + 2\tilde{Q}^{(2)}_{SRR,x}, \quad Q^{(3)} = \tilde{Q}^{(3)}_{CR,x} + \tilde{Q}^{(3)}_{SRR,x} + \tilde{Q}^{(3)}_{SRL,x}. \tag{18a,b}$$

If the flow rates $Q^{(i)}$ are given, the $K^{(i)}$ are determined from the system of algebraic equations (17), (18). Alternatively, given $K^{(i)}$ one can determine the flow distribution in the fully developed flow region. The ratio $\gamma = K^{(2)}/K^{(3)}$ may be used to control the flow.

The deviation of any flow quantity from its fully developed value will be called three-dimensional. For example, the three-dimensional pressure $p^{(i)}_{3D}$ and the three-dimensional pressure drop $\Delta p^{(i)}_{3D}$, are defined as follows:

$$p^{(i)}_{3D} = p^{(i)} + xK^{(i)}, \quad \Delta p^{(i)}_{3D} = \lim_{x \to -\infty} \{p^{(i)}_{CR} + xK^{(i)}\}. \tag{19a,b}$$

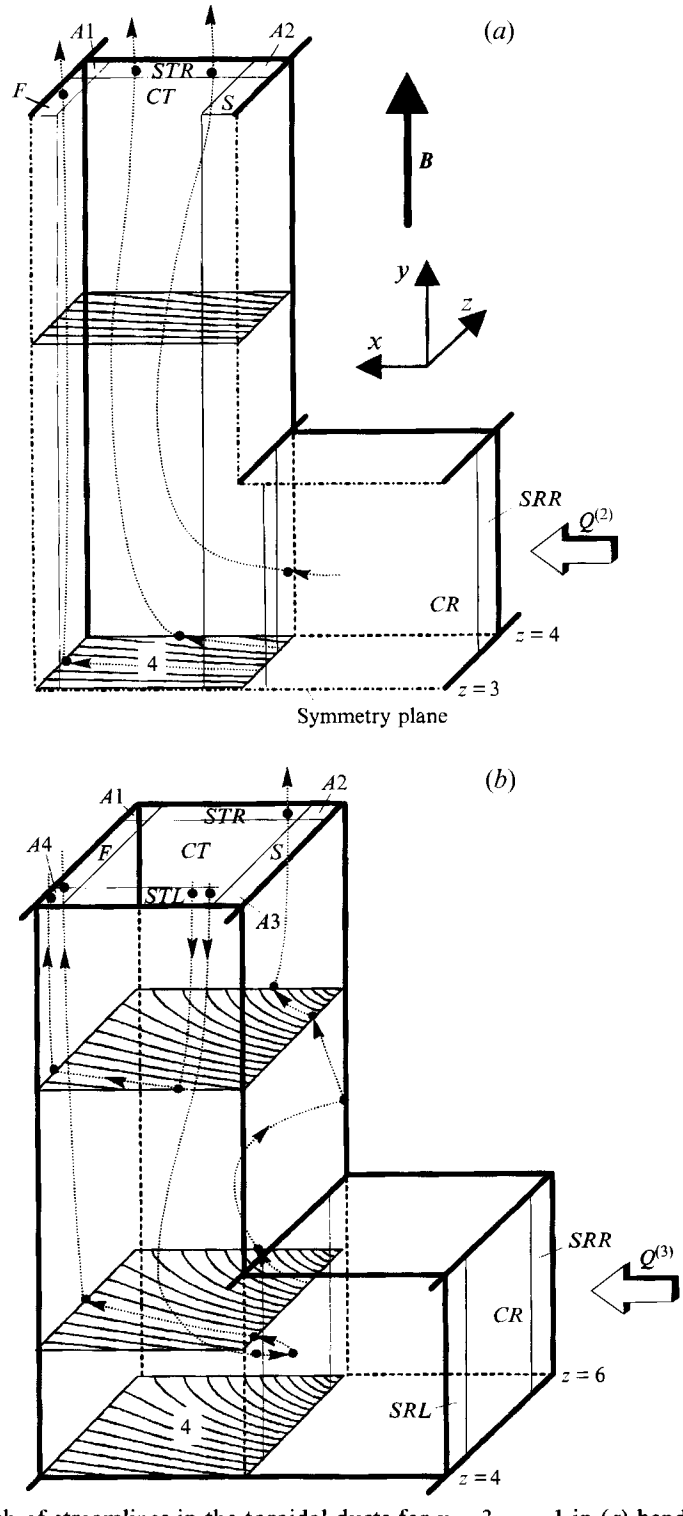

FIGURE 7. Sketch of streamlines in the toroidal ducts for $n = 3$, $\gamma = 1$ in (a) bend 2 and (b) bend 3. Solid circles indicate locations where the fluid leaves one flow subregion and enters another one.

Flow with equal fully developed pressure gradients

It is convenient to consider first the flow with equal fully developed pressure gradients ($\gamma = 1$). Some preliminary results for this case have been presented in a conference paper (Molokov & Stieglitz 1994).

Far from the junction the flow in the radial ducts is fully developed, and since the difference between pressure gradients in all bends in this region is zero, there is no excess current that would flow in the dividing walls in the $\pm y$-direction (Molokov 1993). The induced core current flowing in planes $x = \text{const.}$ passes through all channels unchanged and returns back through the sidewalls $z = z^{(1,4)}$, and the Hartmann walls (black arrows in figure 3). As the flow approaches the junction the absolute value of the electric potential decreases both inside the fluid and in the walls, so that in the radial ducts the three-dimensional currents circulate close to the junction with the x-component essentially non-zero (figures 4 and 5). In a duct with no dividing walls the three-dimensional core current would flow from the wall $z = z^{(1)}$ to the wall $z = z^{(4)}$ (dashed line in figure 4) and then would close the loop in the walls of the toroidal ducts (black arrows in figure 4). Since the dividing walls $z = z^{(2,3)}$ are present, part of the three-dimensional current induced in the radial duct of bend 2 flows along these walls in the $\pm x$-direction as shown in figure 4 (white arrows). As a result, close to the junction the second three-dimensional current loop appears, which involves only the walls of the toroidal duct of bend 2. Thus the three-dimensional pressure drop induced by these currents is higher in bend 2 than in bend 3 (cf. table 1) and more than double that induced in a single bend ($n = 1$).

For $z > \frac{1}{2}L$ part of the three-dimensional current that reaches the bottom walls 4 of the toroidal ducts may eventually leave them to enter the cores *CT*, where it flows parallel to the magnetic field lines since the other two components of the current vanish to order 1 (equation (7*f*)).

The core velocity in the radial ducts as $x \to -\infty$ is constant, equal to 0.926, and is the same for all bends (cf. equation (7*a*) and figure 6). Since the side layers at the walls $z = z^{(1,4)}$ carry a non-zero volume flux, while $\tilde{Q}^{(2)}_{SRR,x} = \tilde{Q}^{(3)}_{SRL,x} = 0$, the total volume fluxes in bends 1 and 3 are higher than in bend 2 (equations (17), (18)). For $c = 0.4$ the flow rates are $Q^{(2)} = 3.706$, $Q^{(1,3)} = 4.147$ and $\tilde{Q}^{(3)}_{SRR,x}/Q^{(3)} = 0.107$. As the fluid approaches the junction, the three-dimensional currents change the uniform core velocity profile and the flow partition between the cores and the parabolic layers.

Consider bend 2 for $z > \frac{1}{2}L = 3$. The flow pattern here is qualitatively the same as in a single bend (cf. the Introduction and figure 7*a*) with the difference that there are no jets at the sidewalls as $x \to -\infty$. Closer to the junction the axial potential gradient creates a higher core velocity at the wall $z = z^{(3)}$ than in the duct centre (figure 6), while the wall current supports a non-zero volume flux carried by layer *SRR* in the x-direction. This requires a flow redistribution between the core and the layer which is created by the positive z-component of the core velocity. However, the volume flux carried by layer *SRR* is small. At the junction it carries less than 1 % of the total volume flux in bend 2.

The fluid that enters the toroidal duct from layer *SRR* enters layer *STR*. However, this stream does not reach layer *F* along wall 3 as in the corresponding flow in a single bend owing to the weakness of the x-component of the velocity within layer *STR* (figure 8). Instead, it turns in the y-direction within this layer.

For the fluid approaching the toroidal duct from the core *CR* the internal layer *I* appears to be a permeable wall. Part of the fluid from the core *CR* penetrates into the core *CT*, while the other part turns inside layer *I* in the z- and y-directions and flows

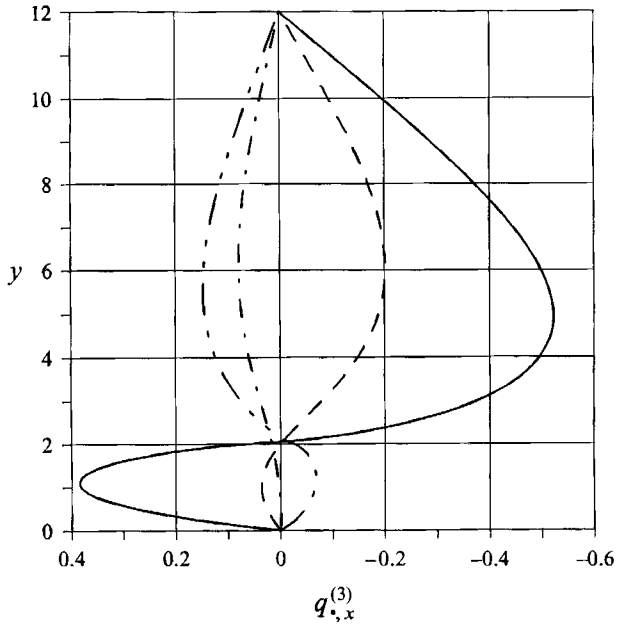

FIGURE 8. Local flow rates carried by layers *STR* and *STL* at the corners *A*1–*A*4 in the x-direction for $n = 3$, $\gamma = 1$: $q^{(3)}_{STR,x}(x = 0)$ (——), $q^{(3)}_{STR,x}(x = d)$ (------), $q^{(3)}_{STL,x}(x = 0) = -q^{(2)}_{STR,x}(x = 0)$ (–·–·–·–), $q^{(3)}_{STL,x}(x = d) = -q^{(2)}_{STR,x}(x = d)$ (–·–·–).

around the core *CT* in the parabolic layers. This flow redistribution results in a jump in the core velocity across layer *I* (figure 6). The fluid that enters the core *CT* at $x = +0$ is distributed between layers *STR* and *F*. Since the y-component of the core velocity vanishes, the fluid flows in the planes $y = \text{const.}$, following the isolines of $\phi_4^{(2)}$. In the major part of the toroidal duct of bend 2 the isolines are nearly straight lines $z = \text{const.}$ Effectively, most of the fluid from the core *CT* enters layer *F* and creates a jet within this layer in the y-direction. There is a volume flux from layer *F* into layer *STR* via the corner *A*1, so that layer *F* loses part of the volume flux as the flow develops with y. However, the volume flux into layer *F* from the core is considerably higher, so that the total volume flux carried by layer *F* monotonically increases with y (figure 9). At $y = l$ layer *F* carries more than 70% of the total volume flux in bend 2. The volume fluxes carried by layers *I* and *STR* also increase with y, while that carried by layer *S* decreases owing to continuous pumping of the fluid from this layer and distribution of it between layers *F* and *STR*. The pumping in the toroidal duct is very intensive, so that layer *S* carrying about 50% of the total volume flux in bend 2 at $y = 2$ loses all of it to the other layers as the flow develops with y. There is a weak recirculatory flow in the toroidal duct for $8.7 < y < 15.3$ associated with a negative volume flux carried by layer *S* in this region. This recirculatory flow is exactly the same as that discussed in MB94. In addition, a helical type of flow pattern is possible at the corner *A*2 (not shown in figure 7*a*), which is determined by the combined effect of flow from layer *STR* into layer *S* for $y > 2$ (figure 8) and pumping of fluid from layer *S* into layer *STR* through the core *CT*.

Consider the flow in bend 3. The flow pattern here is more complex (figure 7*b*). The fluid that enters the core *CT* from the core *CR* is distributed between layers *F* and *STR* as in bend 2. The amount of fluid that enters layer *STR* in bend 3 is significantly higher than that in bend 2.

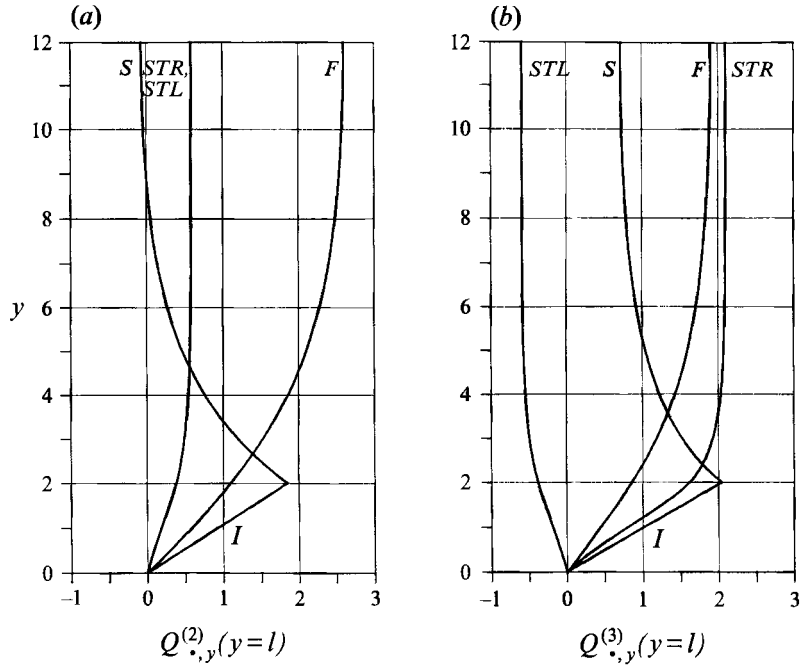

FIGURE 9. Flow distribution in the toroidal ducts for $n = 3$, $\gamma = 1$ in (*a*) bend 2 and (*b*) bend 3.

Consider now the events at the wall $z = z^{(4)} = 6$. In the region of fully developed flow, far from the junction there is a jet at this wall. Close to the junction the axial potential gradient strengthens this jet. As a result there is a very strong jet from layer *SRR* into layer *STR*, part of which for $y < 2$ even reaches layer *F* (figure 8). In layers *STR* and *F* the fluid turns in the y-direction. For $y > 2$ mass exchange between layers at the corners *A*1 and *A*2 changes sign. As a result there is a weak flow from layer *F* into layer *STR* at the corner *A*1 and a significant flow from layer *STR* into layer *S* at the corner *A*2. The resulting flow pattern may involve a helical type of flow as shown in figure 7(*b*). The intensity of this helical flow is much higher than in the toroidal duct of bend 2 at the corner *A*2.

Concerning the wall $z = z^{(3)} = 4$, the three-dimensional current in this wall causes equal and opposite jets in the layers to both sides of it. This leads to jets in layer *SRL* in the $-x$-direction and in layer *STL* in the $-y$-direction. The negative volume flux in these layers is associated with a recirculatory flow. The intensity of the reversed flow has a maximum at $y = l$ and monotonically decreases as y decreases (figure 9*b*). This means that part of the fluid, carried by layer *STL* in the $-y$-direction, leaves the layer to the core *CT* and then flows to layer *F*. This recirculatory flow is similar to that present in MB94 and that in bend 2, but the layers involved are different. In addition, this flow occupies the whole region $0 < y < l$ close to wall 9 and even extends into the radial duct. Indeed, there is a volume flux from layer *STL* into layer *SRL* at $x = 0$ (figures 7*b* and 8). Since there is no reversed flow as $x \to -\infty$, all the fluid from layer *SRL* enters the core *CR*, where the x-component of velocity is positive, and then penetrates into the core *CT* through layer *I*.

In the whole toroidal duct there is pumping of the fluid from layers *S* and *STL* and distribution of it between layers *F* and *STR* through the core. As a result of this pumping the volume fluxes carried by layers *S* and *STL* decrease with increasing y, while those carried by layers *F* and *STR* increase with y (figure 9*b*).

Flow with non-equal fully developed pressure gradients

The flow distribution and the pressure drop depend on the ratio of $K^{(2)}$ to $K^{(3)}$, so that γ may be successfully used to control both global and local flow characteristics. Variation of γ may be achieved by varying the flow rates $Q^{(i)}$. We recall that the total volume flux carried by the system of bends remains fixed, and is equal to 12.

If $Q^{(2)} > 3.706$, then $\gamma > 1$ and the amount of current induced by the core CR in bend 2 in the region of fully developed flow becomes higher than that induced in bends 1 and 3. An excess core current closes its loop in the dividing walls $z = z^{(2,3)}$ and in the top and bottom of the duct 2 (white arrows, dashed lines in figure 3). This current creates positive jets at the dividing walls of duct 2 and negative jets at these walls in ducts 1 and 3 as $x \to -\infty$.

The path of three-dimensional currents is exactly the same as for $\gamma = 1$, but the increase in γ leads to a strengthening of the effects described for $\gamma = 1$. The flow rates carried by all the parabolic layers in the toroidal duct of bend 2 increase, while those carried by layers in bend 3 decrease (figure 10). However, the decrease of the flow rate $Q^{(3)}_{F,y}$ is insignificant. The recirculatory flow in bend 3 extends into the radial duct for a longer distance than for $\gamma = 1$. Since the problem (2)–(6) is linear with respect to $Q^{(2)}$ all flow characteristics vary linearly with it, as does Δp_{3D} in both bends (figure 11).

For $Q^{(2)} = 4$ the flow rates in all the bends become equal, while $K^{(2)} = 0.280$, $K^{(3)} = 0.258$, $\gamma = 1.085$, $\Delta p^{(2)}_{3D} = 0.434$, $\Delta p^{(3)}_{3D} = 0.319$, i.e. for equal flow rates both the fully developed and the three-dimensional pressure drops are higher in the middle bend than in the outer one.

For $Q^{(2)} > 4$ the reverse flow in layer S of bend 2 disappears, while for $Q^{(2)}$ higher than about 8 it appears in layer S of bend 3.

An interesting situation occurs when the middle duct carries all the volume flux ($Q^{(2)} = 12$, $Q^{(3)} = 0$, $K^{(2)} = 0.705$, $K^{(3)} = 0.068$, $\gamma = 10.368$). Although the volume flux in bend 3 is zero, the fluid in this bend is not stagnant. In fact, the recirculatory flow in this case is the most intensive in the whole range $0 \leqslant Q^{(2)} \leqslant 12$. The reason is that a negative jet exists in bend 3 in layer SRL. Since $Q^{(3)} = 0$ this reversed flow must be balanced by a positive volume flux in the core CR and in layer SRR, which requires a small but non-zero value of $K^{(3)}$. The same arguments apply to the toroidal duct of bend 3, where a negative jet in layer STL exists. A negative jet in layer S also contributes to the recirculatory flow.

To get stagnant fluid in the core CR and layer SRR of bend 3 as $x \to -\infty$ one has to assume that $K^{(3)} = 0$ ($K^{(2)} = 3c/(1+c) = 0.857$, $\gamma \to \infty$, $Q^{(2)} = 14.857$, $Q^{(3)} = -1.429$). There is a negative flow rate in bend 3, since the negative volume flux carried by layer SRL cannot be balanced. The flow pattern in the toroidal duct is similar to that for $Q^{(3)} = 0$, so that the discussion in the previous section still applies. It is worth noting that $K^{(2)}$ is exactly three times larger than in the Hartmann flow (one-dimensional flow between parallel walls perpendicular to the field).

For $Q^{(2)} < 3.706$ ($\gamma < 1$) the amount of current induced in the fully developed flow region in bends 1 and 3 is higher than that induced in bend 2. These excess currents again flow in the dividing walls but in directions opposite to those for $\gamma > 1$ (white arrows, dotted lines in figure 3). Therefore the direction of the jets at the dividing walls changes sign. The volume fluxes carried by the parabolic layers in the toroidal duct of bend 2 decrease while those in bend 3 increase with decreasing $Q^{(2)}$ (figure 10). The transition of a flow with $\gamma = 1$ to one with $\gamma < 1$ is quite interesting. When γ becomes slightly lower than 1, the jets at the dividing walls as $x \to -\infty$ are very weak. They are negative in bend 2 and positive in bends 1 and 3. However, closer to the junction the

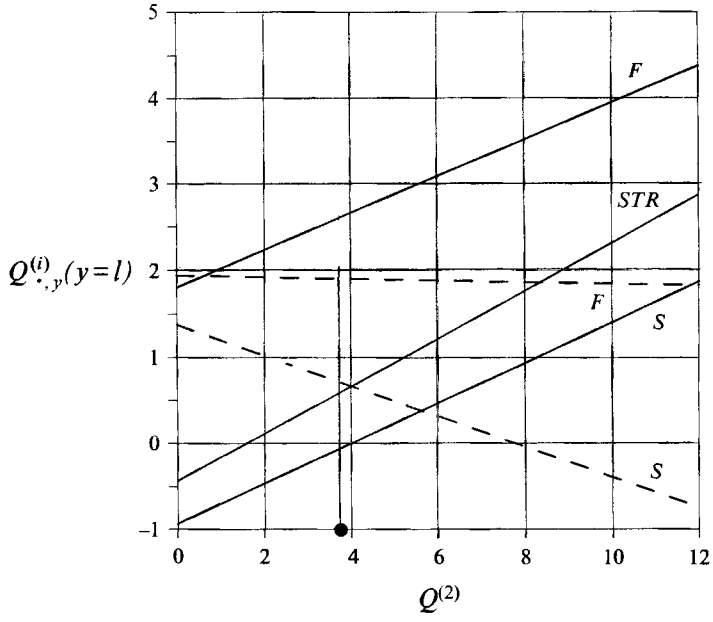

FIGURE 10. Variation of flow distribution in the toroidal ducts at $y = l$ with $Q^{(2)}$ for $n = 3$ in bend $i = 2$ (——) and in bend $i = 3$ (------). The case of equal fully developed pressure gradients is marked with the solid circle.

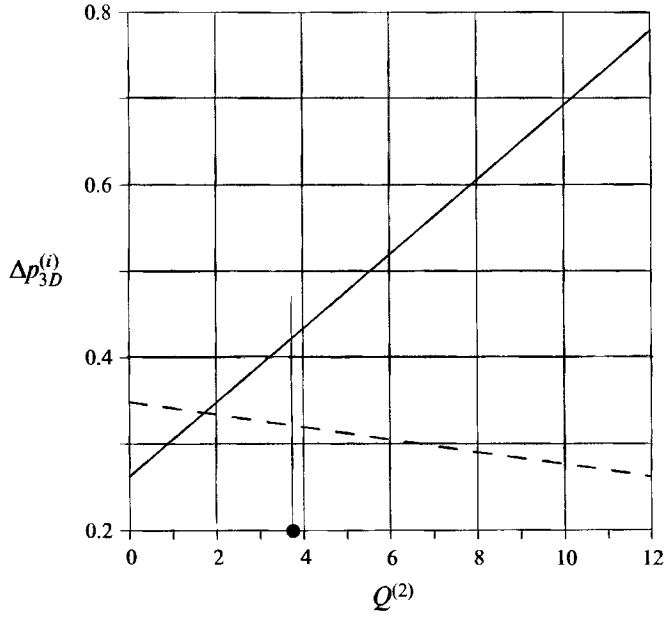

FIGURE 11. Variation of the three-dimensional pressure drop with $Q^{(2)}$ for $n = 3$ in bend $i = 2$ (——) and in bend $i = 3$ (------). The case of equal fully developed pressure gradients is marked with the solid circle.

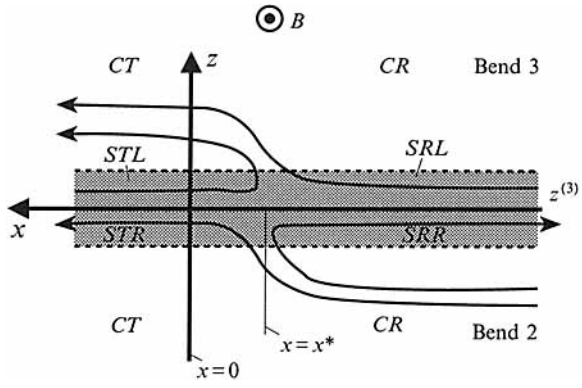

FIGURE 12. Flow paths at the dividing wall $z = z^{(3)}$ for $n = 3$ and for γ slightly lower than 1.

jets are opposite, i.e. they are still in the same direction as for $\gamma = 1$. This means that in bend 2 for x lower than some x^*, part of the fluid that leaves the core CR to enter layer SRR flows backward within this layer (figure 12). For $x > x^*$ the fluid from the core CR enters layer SRR and then the toroidal duct. In bend 3, for $x < x^*$ the fluid in layer SRL leaves it to enter the core CR and then enters the toroidal duct, while for $x > x^*$ the fluid enters layer SRL from the toroidal duct, then leaves this layer to enter the core CR and then enters toroidal duct again. The latter flow path clearly belongs to a recirculatory flow discussed above for $\gamma = 1$.

When γ decreases further, x^* increases and finally is shifted into the toroidal duct. When γ becomes significantly lower than 1 (for $Q^{(2)}$ lower than about 1.5, figure 10) the jet in the whole layer STR of bend 2 becomes negative, while that in layer STL of bend 3 becomes positive. Thus, a reversed flow from the radial duct of bend 2 for $y > l$ into that for $y < l$ becomes possible within layer STR (see also figure 16 in MB94). The recirculatory flow in bend 2 strengthens and involves two vortices: one for $z > \frac{1}{2}L$ and the other by symmetry for $z < \frac{1}{2}L$. The recirculatory flow in bend 3 disappears.

4.2. *Wide bend with no dividing walls*

As has been noted in the previous Section, for $\gamma = 1$ the value of Δp_{3D} in a system of three bends is more than double that in a single U-bend. The natural question arises of whether there is a limit for Δp_{3D} as the channel number increases. The main reason for increasing the pressure drop is the increase in the total width L of the system of U-bends. Indeed, the solution to (2)–(6) for the wall potential and the core pressure for $n = 1$ (no dividing walls) as $x \to -\infty$ is

$$\phi_5 = -\phi_8 = \frac{\frac{1}{2}L + cy(2-y)}{1 + c + \frac{2}{3}L^{-1}}, \quad \phi_{6,7} = \frac{z}{1 + c + \frac{2}{3}L^{-1}}, \tag{20a, b}$$

$$v_{x,CR} = \frac{1+c}{1 + c + \frac{2}{3}L^{-1}}, \quad K = j_{z,CR}(x \to -\infty) = \frac{c}{1 + c + \frac{2}{3}L^{-1}}. \tag{20c, d}$$

Expressions analogous to (20) are well-known (e.g. Moon & Walker 1990). For $L \gg 1$

$$\phi_5 = -\phi_8 \to \tfrac{1}{2}L(1+c)^{-1}, \quad \phi_{6,7} \to z(1+c)^{-1}, \quad v_{x,CR} \to 1, \quad K \to c(1+c)^{-1}, \tag{21a–d}$$

so that all the volume flux tends to be carried by the core, while the absolute value of the pressure gradient tends to that in the Hartmann flow. The electric potential at the sidewalls 5 and 8 linearly increases with L for sufficiently high L. This potential

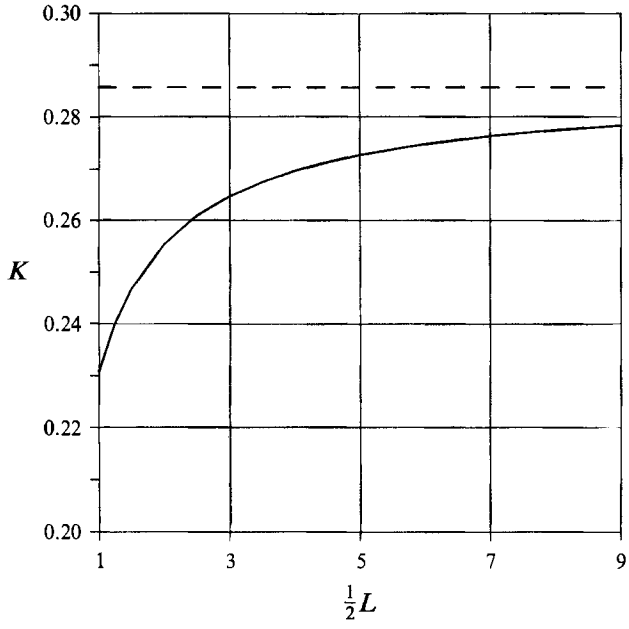

FIGURE 13. Variation of K, the absolute value of the fully developed pressure gradient in a single bend with $\frac{1}{2}L$ or of K in a system of bends (K is equal for all bends) with $n = \frac{1}{2}L$ (solid line). The value of K in the Hartmann flow is shown with dashed line.

difference represents the driving force for the wall currents. In the fully developed flow the core current entering the sidewalls can complete its circuit through the top and the bottom walls of the radial duct only in the planes $x = \text{const.}$, i.e. perpendicular to the main flow direction. Since the distance between the sidewalls L increases, the resistance of the electric circuit also increases linearly with L, and, according to Ohm's law, the magnitude of the wall currents, together with the pressure gradient produced by them, tends to a finite value determined by (21 *d*) (figure 13). In particular, this implies that in a system of straight ducts the pressure drop tends to a finite limit as $L \to \infty$ (Molokov 1993).

Since in the second radial duct of a U-bend at $y > 2l-2$, $x < 0$ the induced voltage difference is of the opposite sign, then close to the junction the three-dimensional current may shortcut along the sidewalls and inside the core of the toroidal duct. If L increases, there is a large electric circuit, shown in figure 1, the resistance of which does not increase with L, since the current that enters the sidewalls has to travel a fixed length of about $2l$ along the toroidal duct. This means that the magnitude of the three-dimensional currents increases linearly with L, together with the three-dimensional pressure drop produced by them (figure 14).

4.3. *Increasing the number of bends*

Consider finally the flow in a wide bend with dividing walls for equal pressure gradients as $x \to -\infty$ so that the flow is consistent with that considered in §4.2. Calculations for $n = 1, 3, 5, 7$ and 9 are presented in figures 14 and 15. Δp_{3D} in the middle and the outer bends is shown in figure 14. $\Delta p_{3D}^{(n+1)/2}$ (middle bend) is higher than that in a single wide bend of corresponding aspect ratio. The reason is that the dividing walls provide an additional path for the electric currents with respect to a single wide bend. All these currents pass through the core CR of the middle bend and induce a high

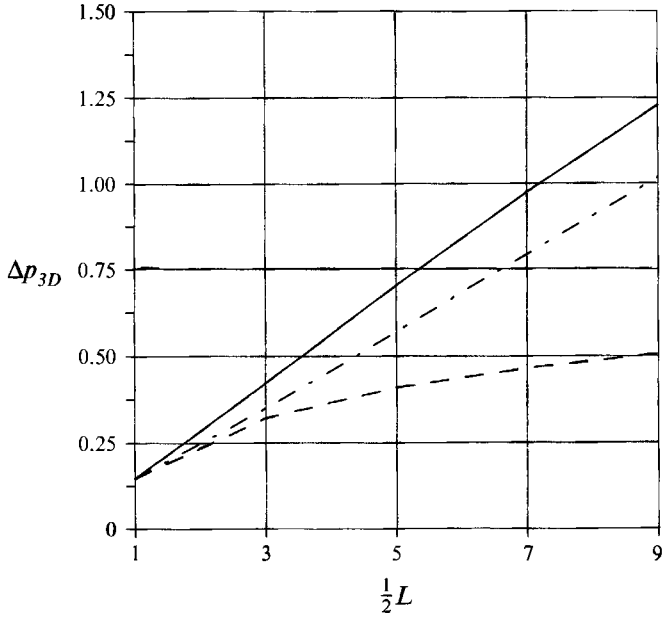

FIGURE 14. Variation of $\Delta p_{3D}^{(1)}$ in a single bend with $\frac{1}{2}L$ (–·–·–), and of $\Delta p_{3D}^{(n+1)/2}$ (middle bend, ——), $\Delta p_{3D}^{(n)}$ (outer bend, – – –) with $n = \frac{1}{2}L$ for odd n.

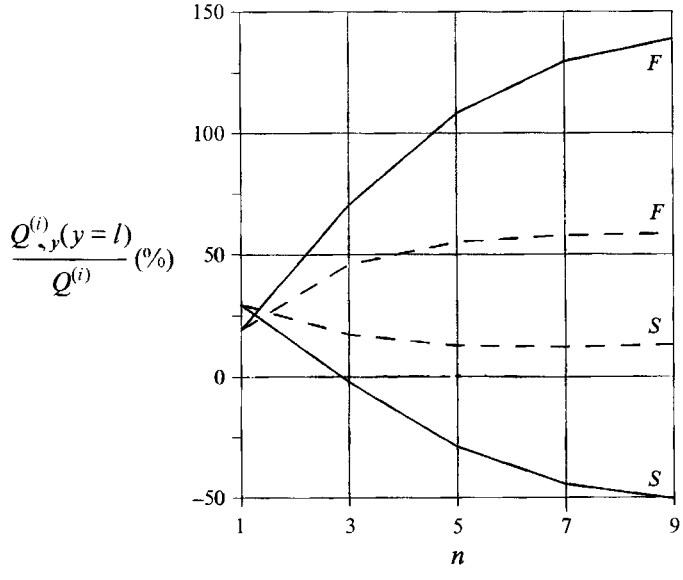

FIGURE 15. Variation of flow rates carried by layers F and S in the y-direction at $y = l$ with n (for odd n) in bend $i = \frac{1}{2}(n+1)$ (middle bend, ——) and in bend $i = n$ (outer bend, ------).

pressure drop there. $\Delta p_{3D}^{(n+1)/2}$ increases almost linearly with L (or n) even for small L, while the slope of $\Delta p_{3D}^{(n+1)/2}$ approaches that for a single wide bend. $\Delta p_{3D}^{(n)}$ (outer bend) is significantly lower than $\Delta p_{3D}^{(n+1)/2}$. From figure 14 it is unclear, however, whether $\Delta p_{3D}^{(n)}$ tends to a finite limit or to infinity. In any case the slope of $\Delta p_{3D}^{(n)}$ is much lower than that of $\Delta p_{3D}^{(n+1)/2}$.

The flow rates carried by all the layers in all bends tend to a finite limit (figure 15).

The limit is almost reached for $n = 9$. The reason is that the flow rate carried by a parabolic layer at an arbitrary wall k of any of the toroidal ducts is proportional to the $\hat{t}_k$-component of the wall current (equation (13)), i.e. only the currents which do not cross the symmetry plane $y = l$ contribute to the flow rates. The magnitude of these currents tends to a constant, because the resistance to them increases linearly with L.

For equal fully developed pressure gradients and for an arbitrary n the flow pattern may be described as follows (cf. main results for $n = 9$ in table 1). In the middle bend $i = \frac{1}{2}(n+1)$ the flow is the same as that discussed in §4.1 for $\gamma = 1$. Close to the junction the jets are created in the positive x-direction. In any other bend $i > \frac{1}{2}(n+1)$ there is a negative jet at the left sidewall and a positive jet at the right sidewall. For $n > 3$ in all bends, including the middle one, a recirculatory flow is present the intensity of which increases with n. For given n the location of the recirculatory flow and the volume it occupies both vary from one bend to the other. For example, for $i = n = 9$ in the toroidal duct it involves layers *F*, *STL* and *STR*. It is interesting to note that for $n > 5$ layer *F* in all the bends carries more than 50% of the volume flux, while in the middle bend it carries even more than 100%, i.e. the recirculatory flow is very intensive.

For non-equal fully developed pressure gradients the flow pattern may be deduced from that for $n = 3$. For example, for equal flow rates in bends both the fully developed pressure gradient and the three-dimensional pressure drop are highest in the middle bend and lowest in the outer bend.

For even n the results are qualitatively the same as those for odd n. The difference is that for even n there is a dividing wall $z = z^{(n/2)}$, which is situated at the symmetry plane $z = \frac{1}{2}L$, where the condition $\phi = 0$ holds. Therefore, the currents cross this wall at right angles, while jets in the layers at this wall vanish and two neighbouring bends $i = \frac{1}{2}n$ and $i = \frac{1}{2}n+1$ behave like a single bend of double aspect ratio with the exception that the no-slip condition holds at the dividing wall $z = z^{(n/2)}$. It should be noted that the results for even n would not lie on the same curves as those presented in figures 14 and 15 for odd n.

5. Conclusions

If ducts are electrically coupled via common conducting walls parallel to the magnetic field, current induced in one duct may enter the other ducts and change both the flow pattern and the pressure drop in the whole system of ducts. If the system involves only straight rectangular ducts with fully developed flow the increase in the pressure drop is insignificant. The absolute values of the pressure gradients tend to that in the Hartmann flow and for a wide range of parameter variation increase by no more than 30% of that in a single-duct flow (Molokov 1993).

If the system involves U-bends, where three-dimensional effects are significant, the pressure drop increases linearly with the width L of the system of bends owing to the contribution of the three-dimensional electric currents which circulate close to the junction. This has also been confirmed experimentally (Stieglitz 1994). For sufficiently high L (in fusion blankets $n \approx 40$, $L = 2n \approx 80$, Malang *et al.* 1988) the pressure drop may reach very high values.

The effect of global currents on the flow pattern is expressed in the presence of equal and opposite jets at the dividing walls. In the radial ducts these jets may vanish if the local axial pressure gradients at both sides of a dividing wall are equal. The appearance of the opposite jets in a U-bend geometry is unavoidable unless the dividing walls are very good conductors. The flow pattern in a system of U-bends is a non-trivial combination of the flow in a single U-bend and that in a system of straight parallel

ducts. The pattern may involve helical and recirculatory flows in both radial and toroidal sets of ducts with several type of vortices. The intensity of the vortex and helical motions increases with the number of channels.

Although for equal fully developed pressure gradients as well as for equal flow rates layer F in each bend carries more than 50% of the total volume flux (in most of the bends even more than 100%), which may be favourable for heat removal from the blanket first wall, special attention should be paid to the recirculatory flow. This flow accounts for about 50% of the flow in all the bends, see the flow distribution at $y = l$ for $n = 9$ in table 1. This fluid does not take an active part in convective heat transfer. On the other hand, the recirculatory flow which exists even within the frame of the present inertialess model may provoke large-scale instabilities in inertial flows and lead to an intensive mixing of the fluid within toroidal ducts. This effect, combined with possible instabilities of high-velocity jets in the parabolic layers may lead to favourable heat-transfer conditions. The final answer on whether such conditions are realized should come from experiments performed for blanket-relevant values of M and N. One such experiment (Stieglitz 1994, Stieglitz *et al.* 1994) for $n \leqslant 5$ shows generally good agreement with the present theory for high values of M and N ($\sim 10^3$–10^4). The other series of experiments (Reimann *et al.* 1993, 1994) performed at lower values of N and M (of the order of 10–150 and 100–500, respectively) shows that other types of flow patterns than those presented here may exist. A discussion of inertia effects and implied modifications in the flow model has been given by Molokov, Bühler & Stieglitz (1994).

To eliminate the dramatic increase of the pressure drop with the number of bends and to reduce the amount of the flow involved in a recirculatory motion one has to break or to reduce the loop of global currents. One way is to electrically separate the radial ducts, which generate the currents, by using insulating ceramic layers inside the electrically conducting walls, as is foreseen in the radial–toroidal–radial blanket concept (Malang *et al.* 1988). The other way is to arrange the fluid flow in such a way that the currents in neighbouring bends cancel, or at least do not amplify each other. This may be achieved if the fluid in any two neighbouring bends flows in opposite directions.

This work has been performed in the framework of the Nuclear Fusion Project of the Forschungszentrum Karlsruhe and is supported by the European Communities within the European Fusion Technology Program. The authors are grateful to Dr Leo Bühler for useful discussions on the topic of this paper.

REFERENCES

Hua, T. Q. & Picologlou, B. F. 1991 Magnetohydrodynamic flow in a manifold and multiple rectangular coolant ducts of self-cooled blankets. *Fusion Technol.* **19**, 102–112.

Hua, T. Q., Walker, J. S., Picologlou, B. F. & Reed, C. B. 1988 Three-dimensional magnetohydrodynamic flows in rectangular ducts of liquid-metal-cooled blankets. *Fusion Technol.* **14**, 1389–1398.

Madarame, H., Taghavi, K. & Tillack, M. S. 1985 The influence of leakage currents on MHD pressure drop. *Fusion Technol.* **8**, 264–269.

Malang, S., Arheidt, K., Barleon, L. *et al.* 1988 Self-cooled liquid-metal blanket concept. *Fusion Technol.* **14**, 1343–1356.

Molokov, S. 1993 Fully developed liquid-metal flow in multiple rectangular ducts in a strong uniform magnetic field. *Eur. J. Mech./B Fluids.* **12**, 769–787.

Molokov, S. & Bühler, L. 1993 Numerical simulation of liquid-metal flows in radial-toroidal-radial bends. *Kernforschungszentrum Karlsruhe. Rep.* KfK 5160.

MOLOKOV, S. & BÜHLER, L. 1994 Liquid-metal flow in a U-bend in a strong uniform magnetic field. *J. Fluid Mech.* **267**, 325–352 (referred to herein as MB94).

MOLOKOV, S., BÜHLER, L. & STIEGLITZ, R. 1994 Asymptotic structure of magnetohydrodynamic flows in bends. In *Proc. 2nd Intl. Conf. on Energy Transfer in Magnetohydrodynamic Flows. Aussois, France, 26–30 Sept., 1994*, pp. 473–484.

MOLOKOV, S. & STIEGLITZ, R. 1994 Leakage current effects in magnetohydrodynamic flows. In *Proc. 2nd Intl Conf. on Energy Transfer in Magnetohydrodynamic Flows. Aussois, France, 26–30 Sept., 1994*, pp. 327–336.

MOON, T. J. & WALKER, J. S. 1990 Liquid metal flow through a sharp elbow in the plane of a strong magnetic field. *J. Fluid Mech.* **213**, 273–292.

REIMANN, J., BUCENIEKS, I., DEMENTIEV, S., FLEROV, A., MOLOKOV, S. & PLATNIEKS, I. 1994 MHD-velocity distributions in U-bends, partially parallel to the magnetic field. In *Proc. 2nd Intl Conf. on Energy Transfer in Magnetohydrodynamic Flows. Aussois, France, 26–30 Sept., 1994*, pp. 391–402.

REIMANN, J., MOLOKOV, S., PLATNIEKS, I. & PLATACIS, E. 1993 MHD-flow in multichannel U-bends: screening experiments and theoretical results. *Kernforschungszentrum Karlsruhe Rep.* KfK-5102; see also *Proc. 17th Symp. on Fusion Technology, Rome, Italy, 14–18 September 1992*, vol. 2, pp. 1454–1458.

SMITH, D. L., BAKER, C. C., SZE, D. K. *et al.* 1985 Blanket comparison and selection study. *Fusion Technol.* **8**, 10–44.

STIEGLITZ, R. 1994 Magnetohydrodynamische Strömungen in Ein- und Mehrkanalumlenkungen. PhD thesis, University of Karlsruhe.

STIEGLITZ, R., MOLOKOV, S., BARLEON, L., REIMANN, J. & MACK, K.-J. 1994 MHD-flows in electrically coupled bends. In *Proc. 2nd Intl. Conf. on Energy Transfer in Magnetohydrodynamic Flows. Aussois, France, 26–30 Sept., 1994*, pp. 403–412.